THE JOURNAL OF BIOLOGICAL CHEMISTRY VOL. 286, NO. 44, pp. 38348–38355, November 4, 2011

Stepwise Adaptations to Low Temperature as Revealed by Multiple Mutants of Psychrophilic α-Amylase from Antarctic Bacterium*[S]

Received for publication, June 21, 2011, and in revised form, August 19, 2011 Published, JBC Papers in Press, September 7, 2011, DOI 10.1074/jbc.M111.274423

Alexandre Cipolla[‡1], **Salvino D'Amico**[‡], **Roya Barumandzadeh**[§1], **André Matagne**[§], **and Georges Feller**[‡2]

From the Laboratories of [‡]*Biochemistry and* [§]*Enzymology and Protein Folding, Center for Protein Engineering, University of Liège, B-4000 Liège-Sart Tilman, Belgium*

Background: Cold-adapted enzymes remain catalytically active at low temperatures.
Results: Mutants of a cold-adapted α-amylase stabilized by engineered weak interactions and a disulfide bond have lost the kinetic optimization to low temperatures.
Conclusion: The disappearance of stabilizing interactions in psychrophilic enzymes increases the dynamics of active site residues at low temperature, leading to a higher activity.
Significance: An experimental support to the activity-stability relationships.

The mutants Mut5 and Mut5CC from a psychrophilic α-amylase bear representative stabilizing interactions found in the heat-stable porcine pancreatic α-amylase but lacking in the cold-active enzyme from an Antarctic bacterium. From an evolutionary perspective, these mutants can be regarded as structural intermediates between the psychrophilic and the mesophilic enzymes. We found that these engineered interactions improve all the investigated parameters related to protein stability as follows: compactness; kinetically driven stability; thermodynamic stability; resistance toward chemical denaturation, and the kinetics of unfolding/refolding. Concomitantly to this improved stability, both mutants have lost the kinetic optimization to low temperature activity displayed by the parent psychrophilic enzyme. These results provide strong experimental support to the hypothesis assuming that the disappearance of stabilizing interactions in psychrophilic enzymes increases the amplitude of concerted motions required by catalysis and the dynamics of active site residues at low temperature, leading to a higher activity.

One frequently overlooks that over 80% of the Earth's biosphere is permanently cold (1) but also that these cold biotopes have been successfully colonized by diverse organisms. Psychrophiles are such cold-adapted organisms thriving permanently at temperatures close to 0 °C and are found, for instance, in Antarctica, the Arctic regions, deep sea water, and sediments, or in the permafrost. They include a large range of representatives from all three domains (Bacteria, Archaea, and Eukarya) and are the most abundant extremophiles in terms of biomass, diversity, and distribution (2, 3). The observation of metabolically active bacteria at −20 °C in the brine veins between sea ice crystals illustrates the remarkable adaptations of psychrophiles (4).

Among the numerous adverse effects of low temperature on the cell (1, 5, 6), the major constraint is exerted on enzyme activity, which is exponentially reduced by temperature decreases. In psychrophiles, this constraint is alleviated by the synthesis of cold-active enzymes to maintain metabolic fluxes compatible with life. The prevailing hypothesis assumes that cold-adapted enzymes have acquired a high catalytic activity at low temperature by improving their conformational flexibility at the expense of stability (7–10). It has been shown that the crystal structure of psychrophilic enzymes is characterized by the disappearance of various noncovalent stabilizing interactions, resulting in both an improved dynamics of the enzyme conformation and in a weak stability (11–17). There is indeed a clear decrease in the number and strength of all known weak interactions and structural factors involved in protein stability, from thermophiles, mesophiles to psychrophiles (17–19).

The heat-labile α-amylase (AHA)[3] from the Antarctic bacterium *Pseudoalteromonas haloplanktis* (20) is the best characterized psychrophilic enzyme. It displays striking sequence and structure similarities with its mesophilic homologue from pig pancreas (PPA) (11, 21–23). For instance, all 24 residues forming the catalytic cleft (supplemental Fig. S1) and involved in substrate binding are strictly conserved in both the psychrophilic and the mesophilic homologues (11, 24). This outstanding example of active site identity demonstrates that cold activity is reached without any amino acid substitution in the reaction center. As a consequence, changes occurring elsewhere in the molecule are responsible for the optimization of

* This work was supported by the Fonds de la Recherche Scientifique-Fonds, National de la Recherche Scientifique, Belgium Fonds de la Recherche Fondamentale et Collective Contracts 2.4535.08 (to G. F.) and 2.4530.09 (to A. M.) and the Belgian Program of Interuniversity Attraction Poles initiated by the Federal Office for Scientific, Technical and Cultural Affaires P6/19.
[S] The on-line version of this article (available at http://www.jbc.org) contains supplemental Figs. S1–S5 and Tables S1 and S2.
[1] Fonds pour la Formation à la Recherche dans l'Industrie et dans l'Agriculture fellow during this work.
[2] To whom correspondence should be addressed: Laboratory of Biochemistry, Center for Protein Engineering, Institute of Chemistry B6a, B-4000 Liège-Sart Tilman, Belgium. Tel.: 32-4-366-33-43; Fax: 32-4-366-33-64; E-mail: gfeller@ulg.ac.be.

[3] The abbreviations used are: AHA, heat-labile α-amylase from *P. haloplanktis*; PPA, α-amylase from pig pancreas; DSC, differential scanning calorimetry; GdmCl, guanidinium chloride.

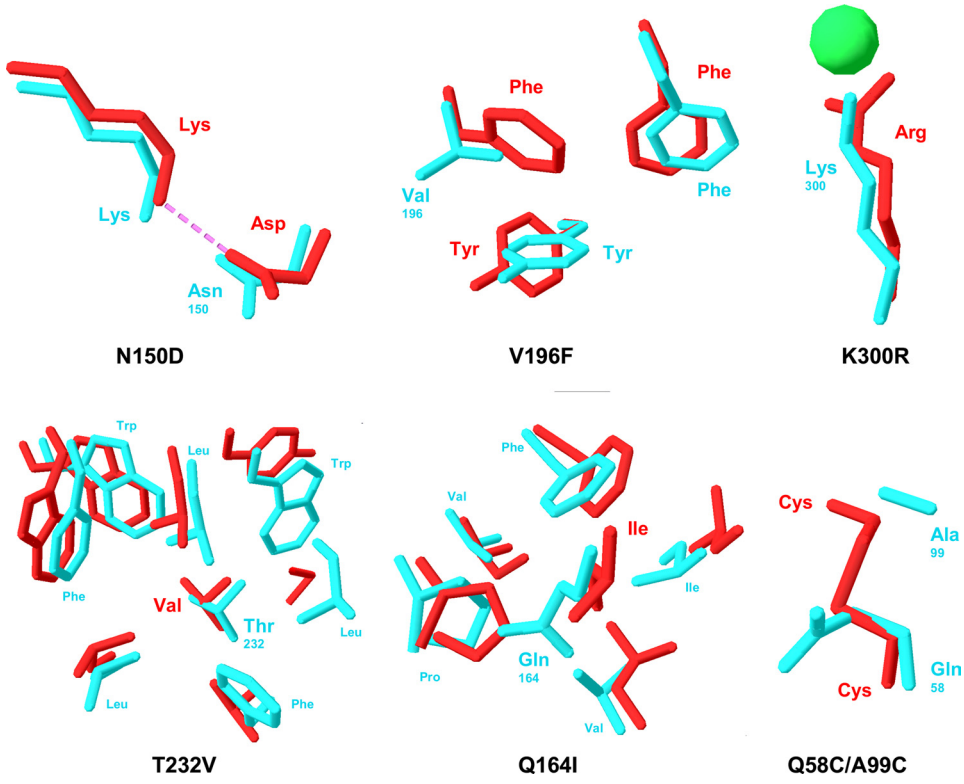

FIGURE 1. **Mutations engineered in the psychrophilic α-amylase AHA (*blue*) based on the structure of the mesophilic homologue PPA (*red*).** The mutation N150D introduces a salt bridge with the corresponding Lys side chain. V196F restores a triple face-to-edge aromatic interaction. K300R provides a bidentate coordination of the chloride ion via short H-bonds as demonstrated by the crystal structure of the single mutant (43). T232V and Q164I increase the apolarity of hydrophobic core clusters (only AHA side chains are labeled for clarity), and the double mutation Q58C/A99C creates a disulfide bond. Protein Data Bank coordinate for AHA is 1AQH and for PPA is 1PPI.

the catalytic parameters at low temperature, by adjustments of the active site residue dynamics. To probe the activity-flexibility-stability hypothesis, numerous mutants of AHA have been constructed, each bearing additional weak interactions mediated by the replacement of a specific residue, as well as a disulfide bond as found in PPA. It has been shown that single amino acid side chain substitutions significantly modify the stability parameters, the cooperativity and reversibility of unfolding, the thermal inactivation rate constant, and the kinetic parameters k_{cat} and K_m (25–27). Here, we report the activity and mainly the stability properties of two stabilized multiple mutants (Fig. 1 and supplemental Fig. S1) of the heat-labile α-amylase AHA as follows: Mut5, bearing five mutations and Mut5CC, also bearing an extra disulfide bond specific to α-amylases from warm-blooded animals (28). The five mutations shared by both multiple mutants have been selected on the basis of the DSC thermograms of single mutants (25) that showed a global stabilization of the protein (higher melting point T_m and calorimetric enthalpy ΔH_{cal}), without evidence for local destabilization (identical or higher temperature of transition start). The lack of interferences between individual mutations, modeled in the crystal structure of AHA, was also checked. These multiple mutants provide clear insights into the structure-function relationships allowing psychrophilic enzymes to fulfill their biochemical functions at low temperatures.

EXPERIMENTAL PROCEDURES

Mutagenesis and Protein Purification—The multiple mutants Mut5 and Mut5CC were constructed by combining restriction fragments of the single mutants and by reverse PCR as described previously (25). The recombinant AHA, Mut5, and Mut5CC were expressed in *Escherichia coli* at 18 °C and purified by DEAE-agarose, Sephadex G-100, and Ultrogel AcA54 column chromatography, as described previously (25). The following parameters were used for calculation: AHA (49,343.1 Da), Mut5 (49,403.2 Da), and Mut5CC (49,410.3 Da) on 453 aa.

Enzyme Assays—α-Amylase activity was recorded using 3.5 mM 4-nitrophenyl-α-D-maltoheptaoside-4,6-*O*-ethylidene as substrate and by the dinitrosalicylic acid method using 1% soluble starch as substrate (25). Microcalorimetric determination of activity toward various polysaccharides and malto-oligosaccharides was performed using an isothermal titration calorimeter as described previously (29).

Differential Scanning Calorimetry—Measurements were performed using a MicroCal VP-DSC instrument at a scan rate of 60 K h^{-1} and under ~25 p.s.i. positive cell pressure. Samples (~2 mg/ml) were dialyzed overnight against 30 mM MOPS, 50 mM NaCl, 1 mM $CaCl_2$, pH 7.2, and, when required, were brought to 1 M 3-(1-pyridinio)-1-propanesulfonate (*i.e.* a non-detergent sulfobetaine) as detailed previously (30). Thermograms of enzyme-acarbose complexes were recorded in the presence of 1 mM acarbose (Bayer). Thermograms were analyzed according to a non-two-state model in which the melting point T_m, the calorimetric enthalpy ΔH_{cal}, and the van't Hoff enthalpy ΔH_{eff} of individual transitions are fitted independently using the MicroCal Origin software (version 7). The magnitude

and source of the errors in the T_m and enthalpy values have been discussed elsewhere (31).

Kinetically driven unfolding was recorded without nondetergent sulfobetaine addition, and the rate constant $k_{u,i}$ was calculated from the relation (32) shown in Equation 1,

$$k_{u,i} = vC_p/\Delta_{cal} - \Delta(T) \quad \text{(Eq. 1)}$$

where v is the scan rate (K s^{-1}); C_p is the excess heat capacity at a temperature T; Δ_{cal} is the total heat of the process, and $\Delta(T)$ is the heat evolved at a given temperature T.

Unfolding Recorded by Intrinsic Fluorescence—Heat-induced unfolding was recorded using an SML-AMINCO model 8100 spectrofluorometer (Spectronic Instruments) at an excitation wavelength of 280 nm and at an emission wavelength of 350 nm (22). GdmCl-induced unfolding was monitored at 20 °C after overnight incubation of the samples at this temperature in 30 mM MOPS, 50 mM NaCl, 1 mM $CaCl_2$, pH 7.2, on an LS50B spectrofluorometer (PerkinElmer Life Sciences) (22). The equilibrium condition was ascertained by recording unfolding as a function of time. Least squares analysis of ΔG^0 values as a function of GdmCl concentrations allowed estimating the conformational stability in the absence of denaturant, ΔG^0_{H2O}, according to Equation 2,

$$\Delta G^0 = \Delta G^0 H_2O - m[\text{GdmCl}] \quad \text{(Eq. 2)}$$

Dynamic Quenching of Fluorescence—The acrylamide-dependent quenching of intrinsic protein fluorescence was monitored as described previously (22). The Stern-Volmer quenching constants K_{SV} were calculated according to Equation 3,

$$F/F_0 = 1 + K_{SV}[Q] \quad \text{(Eq. 3)}$$

where F and F_0 are the fluorescence intensity in the presence and absence of molar concentration of the quencher Q, respectively (33).

Kinetics of Unfolding and Refolding—All kinetic experiments were performed using a Bio-Logic (Claix, France) SFM-3 stopped-flow, coupled with a MOS-200 spectrophotometer and a MPS-51 power supply. Temperature was maintained at 15 °C by a Julabo F30-C thermostated bath. Fluorescence measurements were performed using a 1.5-mm path length cell (FC-15), and the dead time of the apparatus was found to be ~10 ms under all experimental settings. This value was estimated by monitoring the fluorescence of the reduction of dichlorophenolindophenol by ascorbic acid, as described by the manufacturer. All experiments were performed in 30 mM MOPS, 50 mM NaCl, 1 mM $CaCl_2$, pH 7.2, using a protein final concentration of 0.1 mg ml^{-1} (~2 μM). To initiate refolding reactions, unfolded α-amylase (1 mg ml^{-1}) in 3 M GdmCl was diluted 10-fold with aqueous buffer or with GdmCl solutions of varying concentrations to give the desired final concentrations of GdmCl. Conversely, unfolding reactions were initiated by an 10-fold dilution of native α-amylase with the same buffer containing various amounts of GdmCl, to yield final concentrations ranging from 0.3 to 0.9, 0.3 to 1.1, and 0.3 to 1.25 M, for AHA, Mut5, and Mut5CC, respectively. Unfolding and refolding kinetics were followed by intrinsic fluorescence with an excitation wavelength of 280 nm, and total emission above 320 nm was monitored using a high pass filter. For each experiment, 7000 data points were sampled over the entire time course.

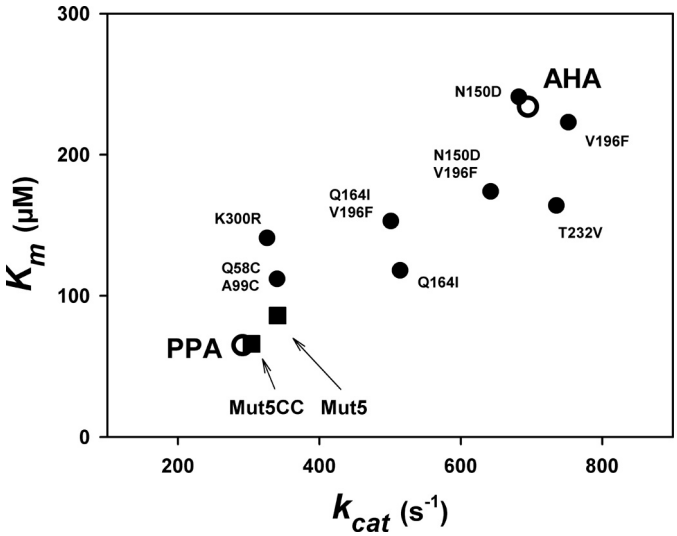

FIGURE 2. **Correlation of kinetic parameters k_{cat} and K_m in the psychrophilic AHA, the mesophilic PPA (*open symbols*), and in single and multiple mutants of AHA.** Activity toward the chromogenic substrate Et-G7-NP at 25 °C. Data are from Refs. 25–27.

Kinetic traces resulting from the accumulation of five identical experiments were analyzed according to the sum of two exponential terms (Equation 4) in the case of refolding and to a simple exponential term (Equation 5) in the case of unfolding.

$$y_t = y_\infty + A_1 \cdot \exp(k_1 \cdot t) + A_2 \cdot \exp(k_2 \cdot t) \quad \text{(Eq. 4)}$$

$$y_t = y_\infty + A \cdot \exp(-k \cdot t) \quad \text{(Eq. 5)}$$

where y_t is the intensity of fluorescence at time t; y_∞ is the signal value for an infinite time; A is the amplitude of the signal associated with rate constant k. The data sets were averaged to obtain the rate constant, and errors were calculated as standard deviations.

The dependence of unfolding and refolding rate constants on denaturant concentration was analyzed according to the following linear relationship (Equation 6) (34, 35),

$$\ln(k_{obs}) = \ln(k_f^{H_2O} \cdot \exp(-(m_{kf}/RT) \cdot [\text{GdmCl}]) + k_u^{H_2O} \cdot \exp((m_{ku}/RT) \cdot [\text{GdmCl}])) \quad \text{(Eq. 6)}$$

where k_{obs} is the rate of unfolding or refolding measured at various GdmCl concentrations, k_f^{H2O} and k_u^{H2O} are the values for folding and unfolding rates, respectively, in the absence of denaturant, and m_{kf}/RT and m_{ku}/RT are proportionality constants, which describe the denaturant dependence. The program Bio-Kine 32 version 4.51 was used for nonlinear least squares analysis of the data.

RESULTS AND DISCUSSION

Activity of the Mutants Mut5 and Mut5CC—The effects of the single, double, and combined mutations on activity toward a chromogenic substrate were described previously (25–27) and are summarized in Fig. 2. The general trend of the muta-

TABLE 1
Relative activity and catalytic constant of Mut5 and Mut5CC on various polysaccharides recorded by microcalorimetry at 25 °C

Substrate	Relative activity				k_{cat}			
	AHA[a]	Mut5	Mut5CC	PPA[a]	AHA[a]	Mut5	Mut5CC	PPA[a]
	%				s^{-1}			
Starch	100	100	100	100	663	352	314	327
Amylopectin	96	94	90	68	636	331	283	222
Dextrin	108	111	112	95	716	391	352	311
Glycogen	74	73	71	59	491	257	223	193
Maltopentaose	69	50	48	145	457	176	151	474
Et-G7-NP	105	97	97	101	642	341	304	330

[a] Data are from Ref. 29.

tions combined to create both multiple mutants is to decrease k_{cat} and K_m concomitantly. Furthermore, a mesophilic like activity was engineered in the multiple mutants Mut5 and Mut5CC as both kinetic parameters are similar to those recorded for the mesophilic homologue PPA.

The specificity of both mutants for various polysaccharides was further investigated by microcalorimetry. Table 1 reports the relative activities of the α-amylases, taking soluble starch, the natural substrate, as a reference. Interestingly, the specificity profile of Mut5 and Mut5CC closely follows that of the parent AHA, indicating that the mode of interaction with these polysaccharides has not been modified. By contrast, comparison of the absolute catalytic constants k_{cat} shows that the activity of the mutants is similar to that of the mesophilic homologue, revealing a less efficient active site.

Fig. 3*b* illustrates the increased stability of both multiple mutants as probed by their heat-induced unfolding recorded by intrinsic fluorescence. Despite their higher thermal stability, there was no significant differences in the apparent optimal temperature for activity, which is recorded near 35 °C (Fig. 3*a*). However, Mut5CC displayed a marked protection against heat inactivation at the upper temperatures. This indicates that the disulfide bond bridging the domains forming the active site cleft contributes to thermal stability of activity in the mesophilic homologue PPA. It should be noted that thermal inactivation above 35 °C (Fig. 3*a*) is recorded before any detectable structural change (Fig. 3*b*). As a result, the active site remains the most heat-labile structural element in both mutants.

Dynamic Fluorescence Quenching—Determination of molecular flexibility requires the definition of the types and amplitudes of atomic motions as well as a time scale for these motions. In this respect, dynamic fluorescence quenching usefully averages most of these parameters into a single signal (33). The structural permeability of the enzymes was investigated by dynamic fluorescence quenching of aromatic residues (dominated by 12 tryptophan residues in AHA and its mutants) by acrylamide. The individual Stern-Volmer plots for AHA and its multiple mutants at 4 and 30 °C are provided in supplemental Fig. S2, and the difference between the slopes of the Stern-Volmer plots at 30 and 4 °C were used to illustrate the difference in structural permeability of the enzymes with an increase in temperature (Fig. 4). The lower slope for Mut5 and Mut5CC indicates a reduced accessibility of aromatic residues relative to AHA, arising from a lower permeability of the mutant structures to the small quencher molecule. This reveals a more compact conformation undergoing reduced micro-unfolding events of the native state and shorter native state fluctuations

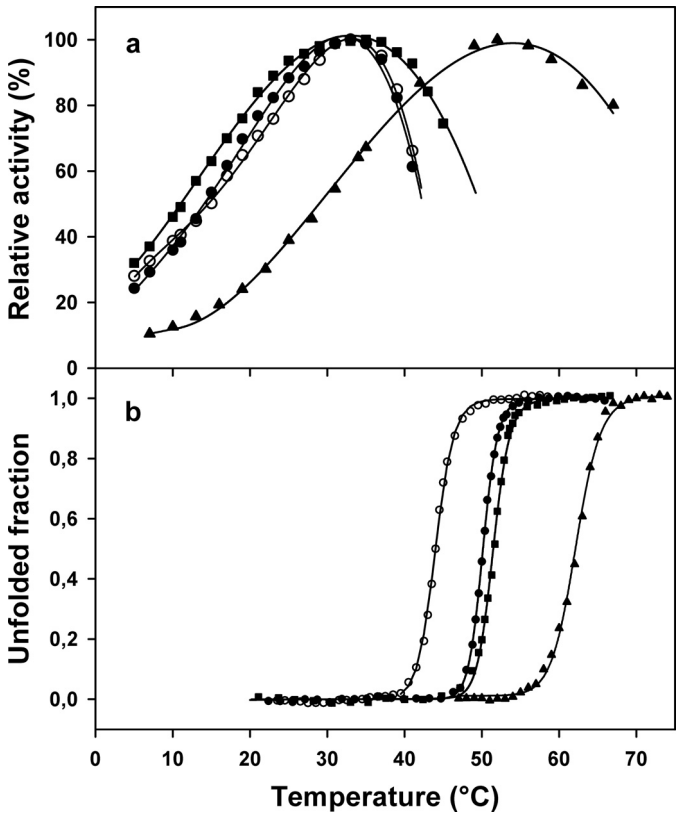

FIGURE 3. **Temperature dependence of activity (*a*) and heat-induced unfolding recorded by fluorescence (*b*).** Data are shown for the psychrophilic AHA (○), the multiple mutants Mut5 (●) and Mut5CC (■), and the mesophilic PPA (▲) (data from Refs. 22, 44). Activity toward starch as substrate. All experiments were performed at similar protein concentrations (5–40 μg/ml).

for both mutants. The flexibility of these proteins and of the mesophilic homologue also correlates with their difference in stability (*i.e.* AHA < Mut5 < Mut5CC < PPA).

Irreversible Unfolding of Stabilized Mutants—Fig. 5 illustrates the correlation between stability of the activity and unfolding reversibility in single and multiple mutants. With the noticeable exception of the disulfide-containing mutant (26), the general trend of the mutations was to protect against heat inactivation but to decrease concomitantly the unfolding reversibility (25). In this respect, both multiple mutants Mut5 and Mut5CC also display mesophilic like properties.

According to the pronounced unfolding irreversibility of both Mut5 and Mut5CC mutants shown in Fig. 5, the kinetically driven stability was analyzed by DSC to determine the rate constant for heat-induced irreversible unfolding, $k_{u,i}$ (32). Such kinetic analysis is not possible for AHA (fully reversible unfold-

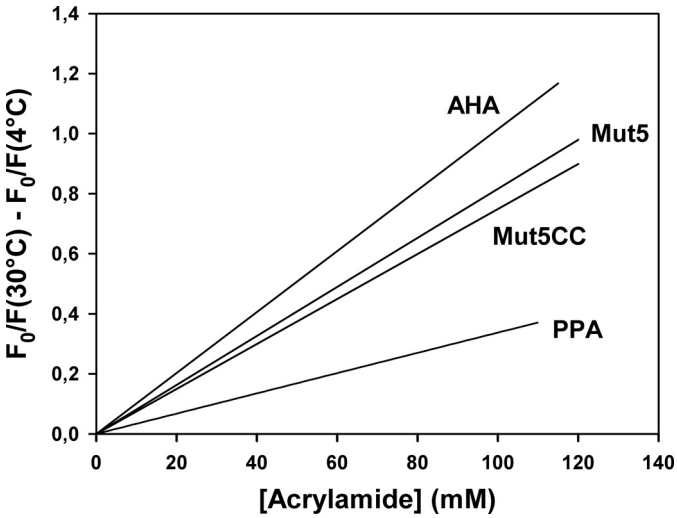

FIGURE 4. **Variation of fluorescence quenching by acrylamide between 4 and 30 °C.** *Graph* was constructed by subtracting the regression lines of Stern-Volmer plots at individual temperatures, as shown in supplemental Fig. S2. Data for the mesophilic PPA (22) are shown at similar temperature intervals.

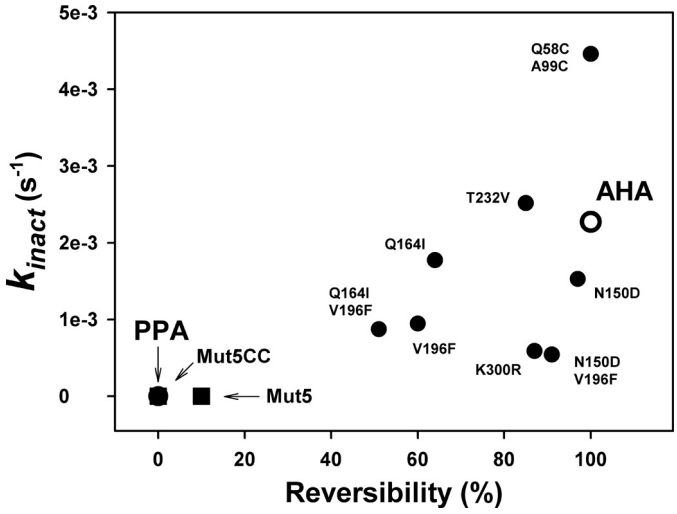

FIGURE 5. **Correlation of stability parameters in the psychrophilic AHA, the mesophilic PPA (*open symbols*), and in single and multiple mutants of AHA.** k_{inact} is the first order rate constant for activity decay at 45 °C, and unfolding reversibility was calculated from two consecutive DSC scans.

ing), and data were obtained from its mutant N12R. The latter displays the same microcalorimetric properties as AHA but only 30% denaturation reversibility (25), ensuring that unfolding is kinetically driven. The temperature dependence of $k_{u,i}$ is shown as an Arrhenius plot in Fig. 6, and the corresponding activation parameters are provided in Table 2.

At an identical temperature of 316 K (43 °C), the rate constants for irreversible unfolding differ by several orders of magnitude, which correspond to higher activation energy barriers ΔG^* in the stabilized mutants (Table 2). Both mutants also display reduced activation enthalpy ΔH^* as calculated from the slope of the plot in Fig. 6. This mainly reflects a lower temperature dependence of irreversible unfolding and therefore a larger resistance toward unfolding in a given temperature interval, as compared with the parent protein AHA. The lower activation enthalpy value of Mut5 (Table 2) arises from its broader

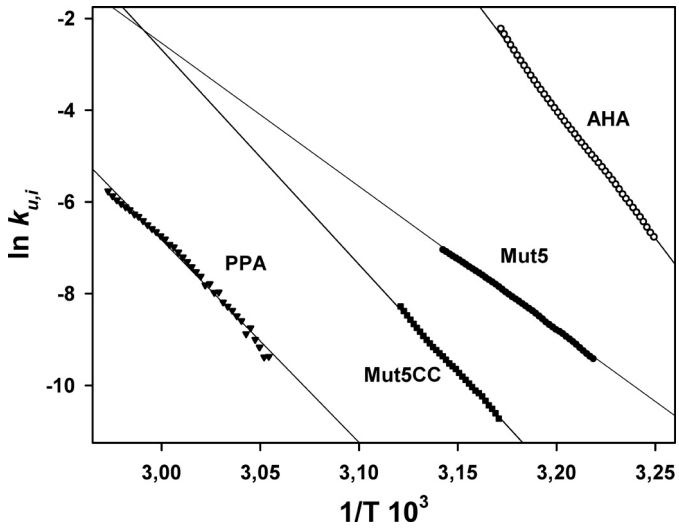

FIGURE 6. **Arrhenius plot of the rate constant for heat-induced irreversible unfolding, $k_{u,i}$.** Data were derived from irreversible DSC endotherms according to Ref. 32 and Equation 1.

TABLE 2

Thermodynamic parameters for heat-induced irreversible unfolding of AHA and its stabilized mutants at 316 K (43 °C)

Protein	$k_{u,i}$	ΔG^*	ΔH^*	$T\Delta S^*$
	s^{-1}	*kcal mol*$^{-1}$	*kcal mol*$^{-1}$	*kcal mol*$^{-1}$
AHA_{N12R}	$1.8 \cdot 10^{-1}$	19.6	112	92
Mut5	$4.6 \cdot 10^{-4}$	23.3	61	38
Mut5CC	$3.1 \cdot 10^{-5}$	25.0	92	67

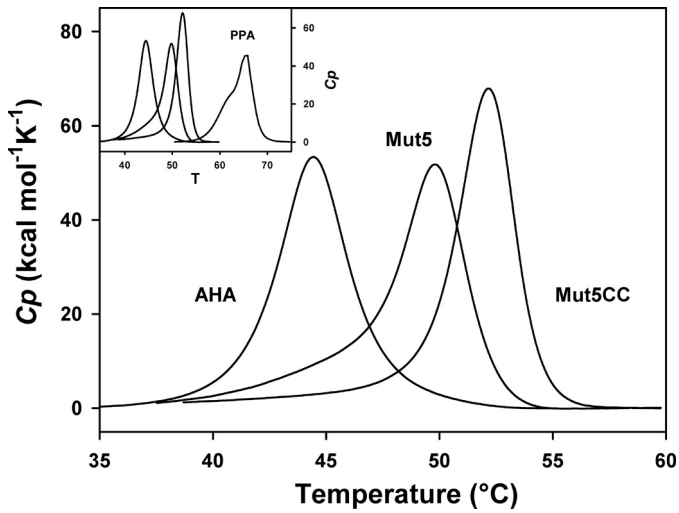

FIGURE 7. **Normalized reversible endotherms of AHA and of its mutants recorded by DSC in the presence of a nondetergent sulfobetaine.** Thermograms were recorded in 30 mM MOPS, 50 mM NaCl, 1 mM $CaCl_2$, pH 7.2, and 1 M 3-(1-pyridinio)-1-propanesulfonate in the case of Mut5 and Mut5CC. Raw data were base line-subtracted and normalized for protein concentration. *Inset,* same graph including the irreversible thermogram of PPA (44).

DSC endotherm (see Fig. 7). The weaker entropic contribution in both mutants can be tentatively explained by a less disordered transition state. In other words, the stabilized mutants would resist against unfolding (before irreversible denaturation) to a larger extent as compared with AHA. As also shown in Fig. 6, PPA unfolds at higher temperatures, which preclude direct comparison. Nevertheless, it is worth noting that Mut5CC tends toward the behavior of PPA in terms of temper-

TABLE 3

Microcalorimetric parameters of thermal unfolding for α-amylases in complex with the pseudosaccharide inhibitor acarbose

The values refer to the differences in T_{max} (top of the transition) and in ΔH_{cal} (area of the transition) with respect to the free enzyme. Activation parameters of the amylolytic reaction at 15 °C are also indicated (27).

	ΔT_{max}	$\Delta\Delta H_{cal}$	$\Delta G^{\#}$	$\Delta H^{\#}$	$T\Delta S^{\#}$
	°C	kcal mol^{-1}	kcal mol^{-1}	kcal mol^{-1}	kcal mol^{-1}
AHA	16.6[a]	115[a]	13.4	8.3	−5.1
Mut5	9.0	53	14.0	11.3	−2.7
Mut5CC	8.3	16	14.0	11.1	−2.9
PPA	16.3[b]	11[b]	14.0	11.5	−2.5

[a] Data are similar to Ref. 22.
[b] Data are from Ref. 22.

ature intervals for irreversible unfolding and ΔH^* (slope of the plot).

Thermodynamic Stability Recorded by DSC—Although heat-induced unfolding of both mutants was irreversible under standard microcalorimetric conditions, we found that addition of the nondetergent sulfobetaine 3-(1-pyridinio)-1-propanesulfonate promotes full unfolding reversibility as illustrated in the supplemental Fig. S3. This compound has been reported to protect unfolded proteins from nonspecific interactions by both charge screening and hydrophobic screening effects (30, 36, 37). Such reversibility of the heat-induced unfolding reaction allowed us to re-investigate the thermodynamic stability (reversible reaction characterized by an equilibrium constant) of Mut5 and Mut5CC, assuming that nondetergent sulfobetaine does not alter the unfolding parameters, as already demonstrated for the parent enzyme AHA (36). Fig. 7 illustrates the normalized DSC thermograms. The thermodynamic parameters of unfolding derived from reversible DSC endotherms are close to those previously obtained under nonreversible conditions (27) and are therefore reported in the supplemental material. As shown in supplemental Table 1, the improved stability of both mutants is characterized by increased melting points (T_m) and calorimetric enthalpies (ΔH_{cal}). This indicates a significant contribution of the engineered interactions in the enthalpic stability of the protein. Furthermore, the stability curves (supplemental Fig. S4) obtained by plotting the Gibbs free energy of unfolding, *i.e.* the work required to disrupt the native state at any temperature (38), clearly illustrate the stability increases brought by the mutations, with, in the case of Mut5CC, values approaching those of the mesophilic homologue PPA.

Stability of α-Amylase-Acarbose Complexes—Acarbose is a pseudosaccharide inhibitor containing an *N*-glycosidic bond and acting as a transition state analogue (39). It has been shown that stabilization induced by acarbose binding closely follows the activation parameters of the amylolytic reaction (22) between the ground state (free enzyme) and the transition state intermediate (enzyme-acarbose complex). The thermograms of AHA and of its mutants were therefore recorded by DSC in the presence of acarbose (supplemental Fig. S5). Table 3 provides the relevant parameters, and the full data set is presented in supplemental Table S2.

Upon acarbose binding, AHA is strongly stabilized, as indicated by the large increase of T_{max} and of the calorimetric enthalpy ΔH_{cal}. It has been argued (22) that this reflects the weak number of interactions to be broken to reach the activated

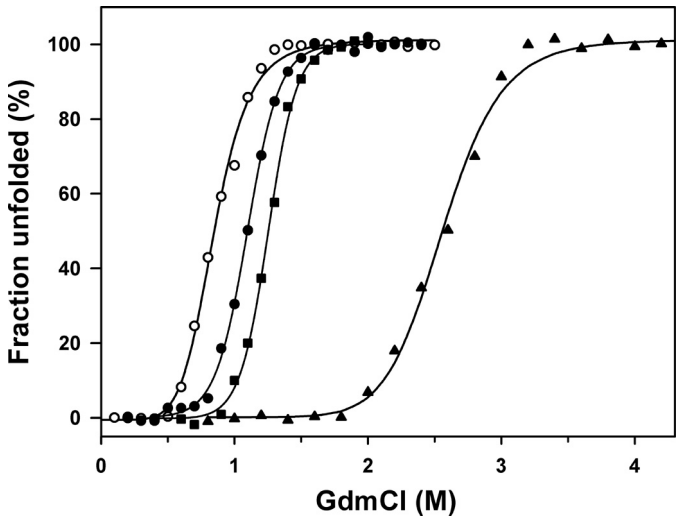

FIGURE 8. **Equilibrium unfolding in GdmCl of AHA and of its mutants as recorded by fluorescence emission.** From *left to right*: AHA (*open circles*), Mut5 (*closed circles*), Mut5CC (*closed squares*), and PPA (*closed triangles*, data from (22)) are shown.

TABLE 4

Equilibrium unfolding parameters in GdmCl of AHA and of its mutants

	$C_{½}$	m	G^0_{H2O}
	M	kcal mol^{-1} M^{-1}	kcal mol^{-1}
AHA[a]	0.86	4.3	3.7
Mut5	1.08	5.1	5.5
Mut5CC	1.25	5.3	6.6
PPA[b]	2.60	2.7	6.9

[a] Data are similar to Ref. 22.
[b] Data are from Ref. 22.

state in the cold-active enzyme (low $\Delta H^{\#}$ in Table 3), which in turn implies large structural motions of the loose free enzyme upon substrate binding (high $\Delta S^{\#}$ in Table 3). It is worth mentioning that Mut5 and Mut5CC are less stabilized by acarbose and display intermediate values with PPA (Table 3). Concomitantly, their activation parameters come close to those of PPA. This is a strong indication that the stabilizing interactions engineered in the mutants directly impair the cold activity optimization of the parent psychrophilic α-amylase.

Equilibrium Unfolding in GdmCl—The resistance toward chemical denaturation using GdmCl was probed by equilibrium unfolding recorded by fluorescence (Fig. 8 and Table 4). Both mutants unfold reversibly at higher GdmCl concentrations ($C_{½}$ values) with respect to AHA and in accordance with their increased thermal stability. The cooperativity of unfolding remains similar to that of AHA, as indicated by the *m* value. Estimation of the conformational stability in the absence of denaturant (ΔG^0_{H2O}) at 20 °C using Equation 2 provides a ratio of 1:1.5:1.8:2 for AHA, Mut5, Mut5CC, and PPA, respectively, in reasonable agreement with the values derived from the DSC stability curves (supplemental Fig. S4).

Kinetics of Unfolding and Refolding—To address the kinetic origin of the gain in stability of the mutants, the folding kinetics in GdmCl were recorded. Indeed, the equilibrium constant $K_{N\text{-}U}$ between the native state N and the unfolded state U ($K_{N\text{-}U}$ = [U]/[N]) is also expressed by the ratio k_{unfold}/k_{fold} of the kinetic constants for unfolding and folding, respectively. As shown in Fig. 9, kinetics of unfolding and refolding were determined

between 0.3 and 2 M GdmCl. Under all conditions, unfolding was found to be a monophasic process, although refolding was a biphasic process comprising a fast phase (~80% amplitude) and a slow phase (~20% amplitude). In the context of our analysis, the corresponding parameters (Table 5) were restricted to the rate constants in the absence of denaturant (k_f^{H2O} and k_u^{H2O}) obtained by linear regression (*dashed lines* in Fig. 9), the corresponding time constants ($\tau = 1/k$), their dependences on the denaturant concentration (m_{kf} and m_{ku}) and, when relevant, the transition midpoint $C_{½}$. Interestingly, the folding rate constants k_f^{H2O} for both phases converge toward very similar values in the three enzymes. By contrast, the unfolding rate constants k_u^{H2O} of both stabilized mutants are reduced as follows: Mut5 unfolds 3.5 times slower and Mut5CC unfolds 13.4 times slower with respect to AHA. It can be concluded that the decreased unfolding rate is the main kinetic determinant of the improved stability in both mutants.

Conclusions—The mutants Mut5 and Mut5CC bear representative stabilizing interactions found in the heat-stable PPA but lacking in the psychrophilic AHA, *i.e.* a salt bridge (N150D), weakly polar interactions (V196F), short H-bonds (K300R), better hydrophobic effect in core clusters (T232V and Q194I), and a covalent disulfide bond (Q58C/A99C) specific to warm-blooded animals (Fig. 1). From an evolutionary perspective, these mutants can be regarded as structural intermediates between the psychrophilic and the mesophilic enzymes. We have shown here that these engineered interactions improve all the investigated parameters related to protein stability as follows: the compactness (as probed by fluorescence quenching), the kinetically driven stability (irreversible heat-induced unfolding), the thermodynamic stability (from DSC endotherms), the resistance toward chemical denaturation (equilibrium unfolding in GdmCl), and the kinetics of unfolding/refolding. Concomitantly to this improved stability, both mutants have lost the kinetic optimization to low temperature activity displayed by the parent enzyme AHA, as demonstrated by their kinetic parameters toward a model substrate (Fig. 2), by their activity toward various polysaccharides and oligosaccharides (Table 1), and by their stability in complex with the transition state analog acarbose (Table 3). These results provide strong experimental support to the prevailing hypothesis (7, 27), *i.e.* the disappearance of stabilizing interactions in psychrophilic enzymes increases the amplitude of concerted motions required by catalysis and the dynamics of active site residues at low temperature, leading to a higher activity but also to a lower substrate binding strength (Fig. 2). We have argued elsewhere that losing stability is apparently the easiest strategy to improve molecular dynamics in cold environments where the selective pressure for stable proteins is lacking (8, 40).

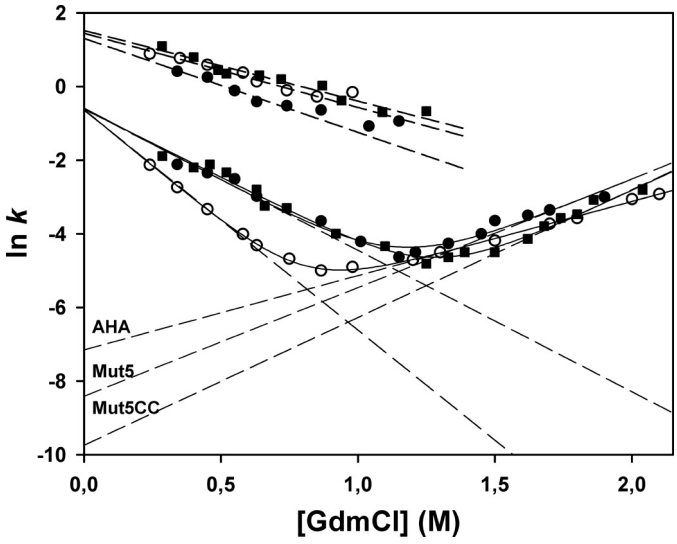

FIGURE 9. **Chevron plots of the GdmCl concentration dependence of the rate constants for unfolding and refolding.** Data for AHA (*open circles*), Mut5 (*closed circles*), and Mut5CC (*closed squares*) are shown. Unfolding rate constants (right arms of the plot) and refolding rate constants (left arms, slow phase) were fitted on Equation 6 (*solid lines*). *Dashed lines* are extrapolations to 0 M GdmCl allowing the determination of k_f^{H2O} and k_u^{H2O}, the folding and unfolding rate constants in the absence of denaturant. Upper data set indicates fast refolding phases.

Two aspects of the present stability studies are also worth comments. (i) The role of disulfide bonds has been frequently debated in the general context of protein stability (26). In the case of Mut5CC, there is an unquestionable contribution of the disulfide to all recorded stability parameters. Furthermore, a fascinating aspect, which deserve further investigations, is the observation that the disulfide has a higher contribution to stability when added to Mut5 than to its effect on AHA alone (26), as far as T_m and ΔH_{cal} variations are concerned. This reflects a very strong cooperativity of stabilizing interactions, rather than a simple additivity, in the maintenance of the native folded state of proteins. (ii) The kinetics of unfolding/refolding of Mut5 and Mut5CC demonstrates that the gain in stability is governed by a slow unfolding rate, although the folding rate remains unchanged (Fig. 9 and Table 5). This perfectly fits with similar experiments performed on hyperthermophilic proteins and aimed at explaining their unusual stability (41, 42). Altogether, these results suggest the occurrence of a transition state on the unfolding pathway, the free energy level of which modulates the stability of proteins adapted to extreme biological tempera-

TABLE 5
Kinetic parameters of unfolding and refolding in GdmCl

	$\ln k_u^{H2O}$	$\ln k_f^{H2O}$	k_u^{H2O}	k_f^{H2O}	τ_u	τ_f	m_{ku}	m_{kf}	$C_{½}$
			s^{-1}	s^{-1}	s	s	kcal M^{-1} mol^{-1}	kcal M^{-1} mol^{-1}	M
Slow phases									
AHA	−7.15	−0.62	7.8e-4	0.53	1282	1.88	1.15	−3.51	0.81
Mut5	−8.41	−0.58	2.2e-4	0.55	4545	1.81	1.67	−2.22	1.14
Mut5CC	−9.74	−0.61	5.8e-5	0.54	17241	1.85	1.97	−2.11	1.26
Fast refolding phase									
AHA		1.44		4.22		0.24		−2.01	
Mut5		1.31		3.69		0.27		−2.55	
Mut5CC		1.26		4.58		0.22		−1.92	

tures. This aspect should stimulate further investigations, using appropriate extremophilic protein models.

Acknowledgments—We thank H. Bichoff (Bayer AG, Germany) for the kind gift of acarbose. The support of the Institut Polaire Français was also appreciated.

REFERENCES

1. Rodrigues, D. F., and Tiedje, J. M. (2008) *Appl. Environ. Microbiol.* **74,** 1677–1686
2. Gerday, C., and Glansdorff, N. (2007) *Physiology and Biochemistry of Extremophiles*, American Society for Microbiology, Washington, D. C.
3. Margesin, R., Schinner, F., Marx, J. C., and Gerday, C. (2008) *Psychrophiles, from Biodiversity to Biotechnology*, Springer-Verlag, Berlin
4. Deming, J. W. (2002) *Curr. Opin. Microbiol.* **5,** 301–309
5. D'Amico, S., Collins, T., Marx, J. C., Feller, G., and Gerday, C. (2006) *EMBO Rep.* **7,** 385–389
6. Casanueva, A., Tuffin, M., Cary, C., and Cowan, D. A. (2010) *Trends Microbiol.* **18,** 374–381
7. Fields, P. A., and Somero, G. N. (1998) *Proc. Natl. Acad. Sci. U.S.A.* **95,** 11476–11481
8. Feller, G., and Gerday, C. (2003) *Nat. Rev. Microbiol.* **1,** 200–208
9. Feller, G. (2010) *J. Phys.: Condens Mat.* **22,** 323101 doi 10.1088/0953–8984/1022/1032/323101
10. Siddiqui, K. S., and Cavicchioli, R. (2006) *Annu. Rev. Biochem.* **75,** 403–433
11. Aghajari, N., Feller, G., Gerday, C., and Haser, R. (1998) *Structure* **6,** 1503–1516
12. Russell, R. J., Gerike, U., Danson, M. J., Hough, D. W., and Taylor, G. L. (1998) *Structure* **6,** 351–361
13. Smalås, A. O., Leiros, H. K., Os, V., and Willassen, N. P. (2000) *Biotechnol. Annu. Rev.* **6,** 1–57
14. Bell, G. S., Russell, R. J., Connaris, H., Hough, D. W., Danson, M. J., and Taylor, G. L. (2002) *Eur. J. Biochem.* **269,** 6250–6260
15. Tehei, M., Franzetti, B., Madern, D., Ginzburg, M., Ginzburg, B. Z., Giudici-Orticoni, M. T., Bruschi, M., and Zaccai, G. (2004) *EMBO Rep.* **5,** 66–70
16. Bae, E., and Phillips, G. N., Jr. (2004) *J. Biol. Chem.* **279,** 28202–28208
17. Coquelle, N., Fioravanti, E., Weik, M., Vellieux, F., and Madern, D. (2007) *J. Mol. Biol.* **374,** 547–562
18. Gianese, G., Bossa, F., and Pascarella, S. (2002) *Proteins* **47,** 236–249
19. Tronelli, D., Maugini, E., Bossa, F., and Pascarella, S. (2007) *FEBS J.* **274,** 4595–4608
20. Médigue, C., Krin, E., Pascal, G., Barbe, V., Bernsel, A., Bertin, P. N., Cheung, F., Cruveiller, S., D'Amico, S., Duilio, A., Fang, G., Feller, G., Ho, C., Mangenot, S., Marino, G., Nilsson, J., Parrilli, E., Rocha, E. P., Rouy, Z., Sekowska, A., Tutino, M. L., Vallenet, D., von Heijne, G., and Danchin, A. (2005) *Genome Res.* **15,** 1325–1335
21. Feller, G., Payan, F., Theys, F., Qian, M., Haser, R., and Gerday, C. (1994) *Eur. J. Biochem.* **222,** 441–447
22. D'Amico, S., Marx, J. C., Gerday, C., and Feller, G. (2003) *J. Biol. Chem.* **278,** 7891–7896
23. Da Lage, J. L., Feller, G., and Janecek, S. (2004) *Cell. Mol. Life Sci.* **61,** 97–109
24. Aghajari, N., Feller, G., Gerday, C., and Haser, R. (1998) *Protein Sci.* **7,** 564–572
25. D'Amico, S., Gerday, C., and Feller, G. (2001) *J. Biol. Chem.* **276,** 25791–25796
26. D'Amico, S., Gerday, C., and Feller, G. (2002) *J. Biol. Chem.* **277,** 46110–46115
27. D'Amico, S., Gerday, C., and Feller, G. (2003) *J. Mol. Biol.* **332,** 981–988
28. D'Amico, S., Gerday, C., and Feller, G. (2000) *Gene* **253,** 95–105
29. D'Amico, S., Sohier, J. S., and Feller, G. (2006) *J. Mol. Biol.* **358,** 1296–1304
30. D'Amico, S., and Feller, G. (2009) *Anal. Biochem.* **385,** 389–391
31. Matouschek, A., Matthews, J. M., Johnson, C. M., and Fersht, A. R. (1994) *Protein Eng.* **7,** 1089–1095
32. Sánchez-Ruiz, J. M., López-Lacomba, J. L., Cortijo, M., and Mateo, P. L. (1988) *Biochemistry* **27,** 1648–1652
33. Lakowicz, J. (1983) *Principles of Fluorescence Spectroscopy*, Plenum Press, New York
34. Khorasanizadeh, S., Peters, I. D., and Roder, H. (1996) *Nat. Struct. Biol.* **3,** 193–205
35. Fersht, A. R. (1999) *Structure and Mechanism in Protein Science: A Guide to Enzyme Catalysis and Protein Folding*, W. H. Freeman & Co., New York
36. Collins, T., D'Amico, S., Georlette, D., Marx, J. C., Huston, A. L., and Feller, G. (2006) *Anal. Biochem.* **352,** 299–301
37. Vuillard, L., Braun-Breton, C., and Rabilloud, T. (1995) *Biochem. J.* **305,** 337–343
38. Privalov, P. (1992) in *Protein Folding* (Creighton, T., ed) pp. 83–126, W.H. Freeman & Co., New York
39. Qian, M., Haser, R., Buisson, G., Duée, E., and Payan, F. (1994) *Biochemistry* **33,** 6284–6294
40. Roulling, F., Piette, F., Cipolla, A., Struvay, C., and Feller, G. (2011) in *Extremophiles Handbook* (Horikoshi, K., ed) pp. 891–916, Springer Verlag, Tokyo
41. Luke, K. A., Higgins, C. L., and Wittung-Stafshede, P. (2007) *FEBS J.* **274,** 4023–4033
42. Perl, D., Welker, C., Schindler, T., Schröder, K., Marahiel, M. A., Jaenicke, R., and Schmid, F. X. (1998) *Nat. Struct. Biol.* **5,** 229–235
43. Aghajari, N., Feller, G., Gerday, C., and Haser, R. (2002) *Protein Sci.* **11,** 1435–1441
44. Feller, G., d'Amico, D., and Gerday, C. (1999) *Biochemistry* **38,** 4613–4619

Supplemental Material to:

Stepwise adaptations to low temperatures as revealed by multiple mutants of a psychrophilic α-amylase from an Antarctic bacterium

Alexandre Cipolla[‡], Salvino D'Amico[‡], Roya Barumandzadeh[§],

André Matagne[§] and Georges Feller[‡1]

From the [‡]Laboratory of Biochemistry and the [§]Laboratory of Enzymology and Protein Folding, Centre for Protein Engineering, University of Liège, B-4000 Liège-Sart Tilman, Belgium

Contents

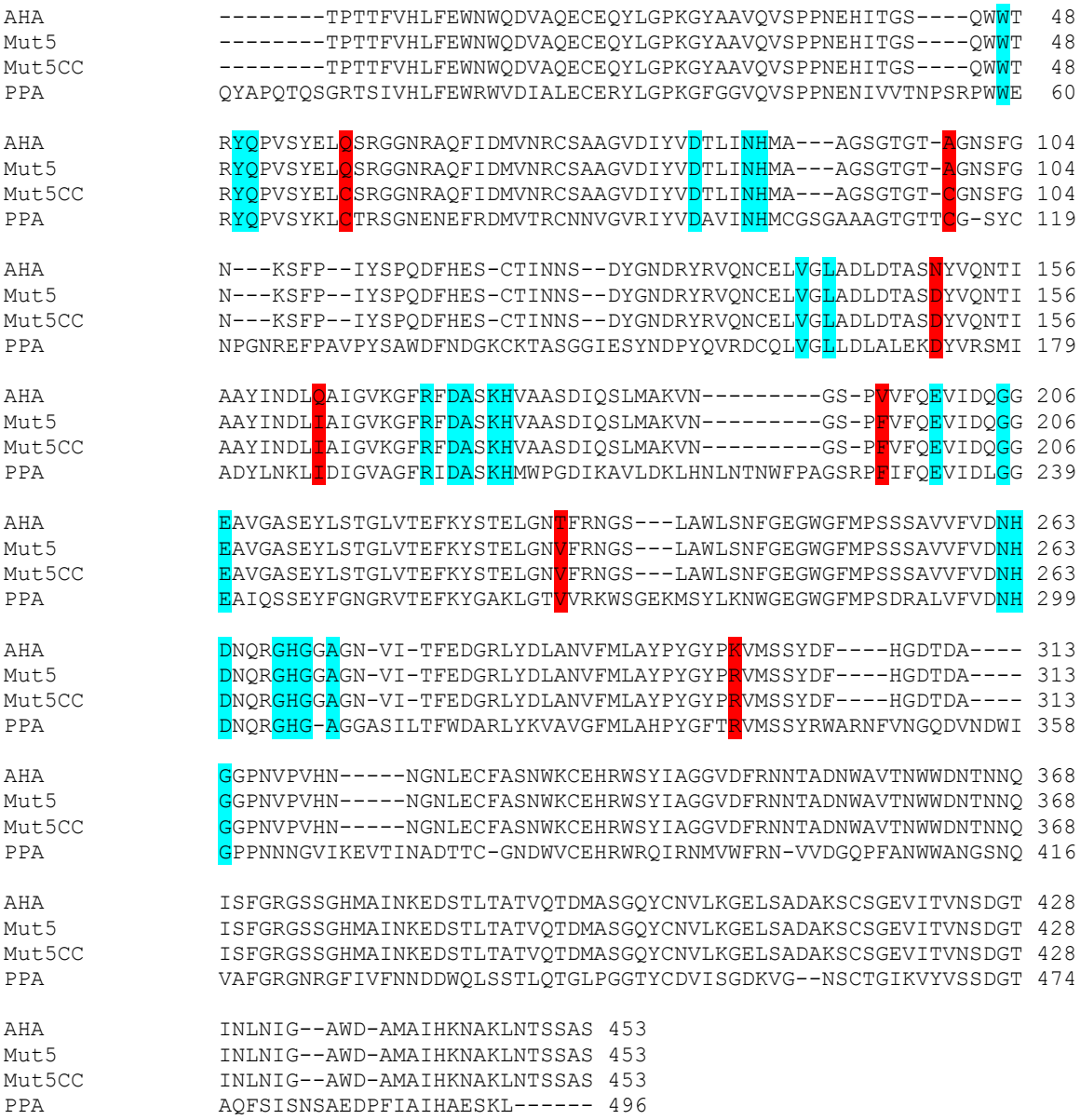

Supplemental Figure S1: Sequence alignment of the psychrophilic AHA, its multiple mutants Mut5 and Mut5CC, and of the mesophilic PPA. The mutations engineered in Mut5 and in Mut5CC are shown in red. The 24 conserved residues forming the active site cleft are shown in blue.

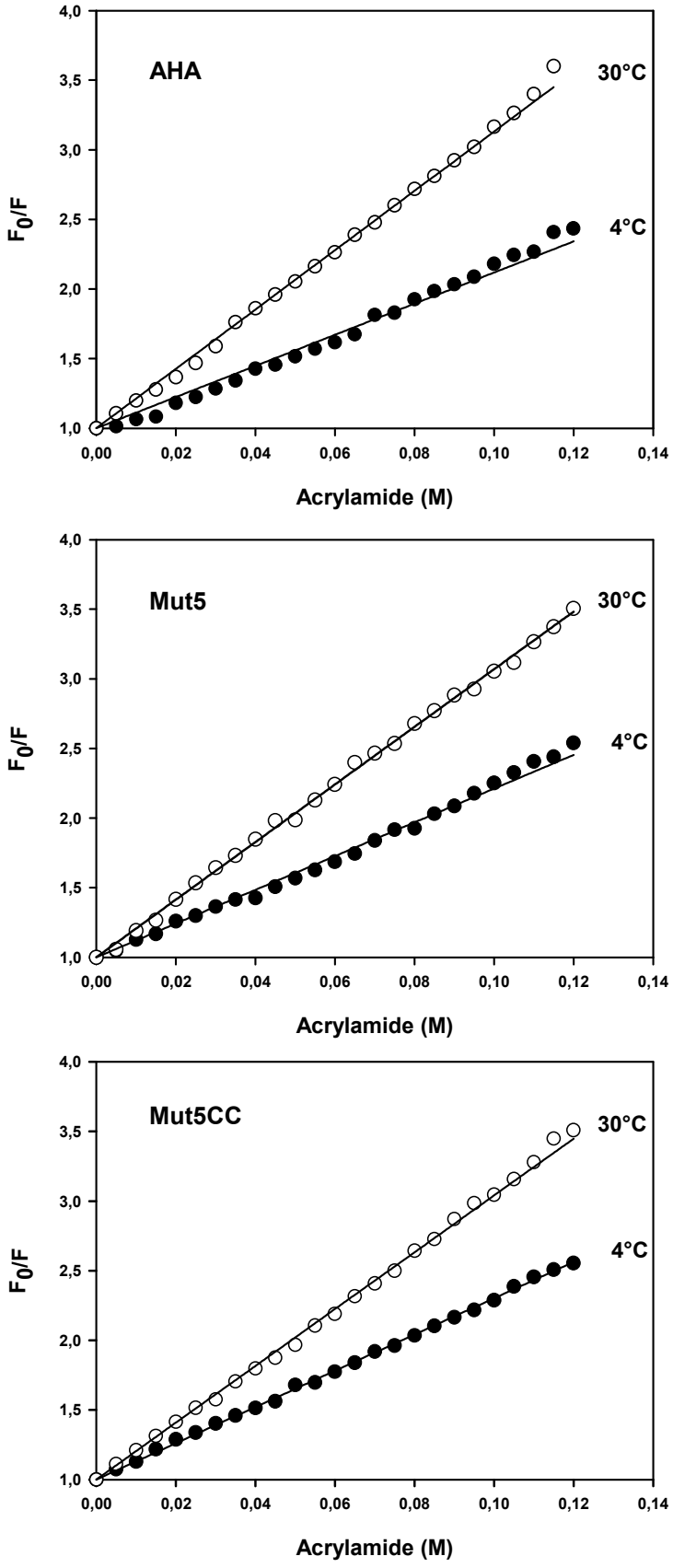

Supplemental Figure S2: Stern-Volmer plots of fluorescence quenching by acrylamide. The quenching constant K_{SV} values corresponding to the plot slope are 11.7, 12.1 and 13.0 M^{-1} at 4°C and 21.3, 20.7 and 20.4 M^{-1} at 30°C for AHA, Mut5 and Mut5CC, respectively.

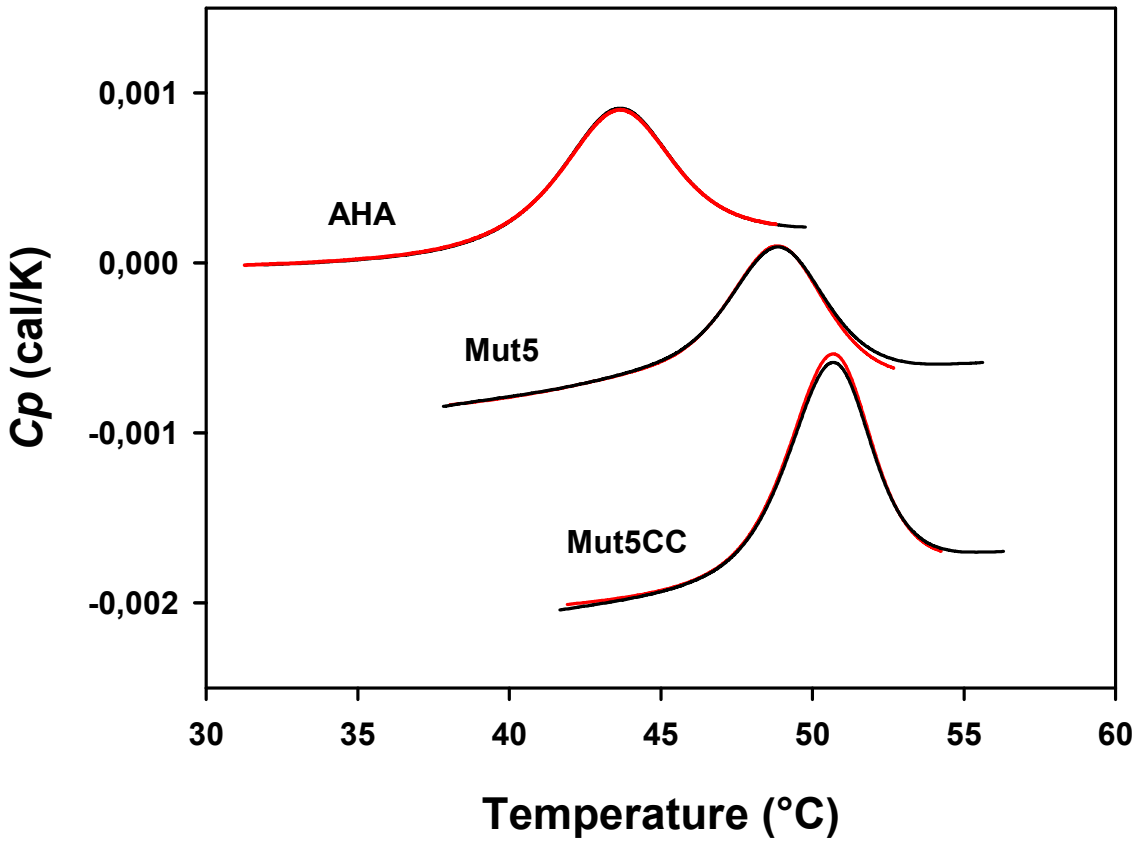

Supplemental Figure S3: Unfolding reversibility of the mutants in the presence of a nondetergent sulfobetaine. Thermograms were recorded in 30 mM Mops, 50 mM NaCl, 1 mM Ca Cl_2, 1 M 3-(1-pyridinio)-1-propanesulfonate, pH 7.2 at a scan-rate of 60 K h^{-1}. Red traces: first up-scans interrupted after completion of the unfolding transition. Black traces: second up-scans performed after sample cooling. Raw data have been displaced along the Y axis for clarity.

Supplemental TABLE S1

Thermodynamic parameters of unfolding derived from reversible DSC endotherms

	T_m °C	ΔH_{cal} kcal mol^{-1}	ΔH_{eff} kcal mol^{-1}	ΔH_{cal} / ΔH_{eff}	Reversibility %
AHA	44.0	214	203	1.05	>99
Mut5	49.7	233	204	1.14[1]	>98
Mut5CC	52.2	280	270	1.04	>98
PPA[2]	65.6	319	--[3]	--[3]	none

[1] despite a ratio close to 1, unfolding deviates from a two-state model as a result of an asymmetric transition
[2] data from (44)
[3] not applicable, biphasic transition

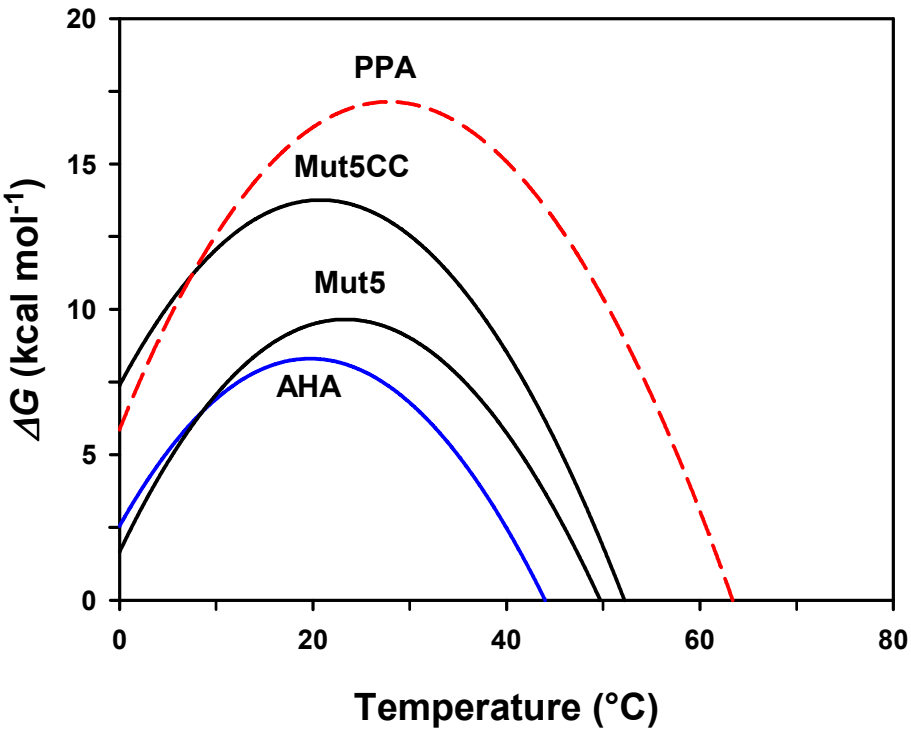

Supplemental Figure S4: Stability curves calculated from DSC data. The Gibbs free energy of unfolding was calculated as described (22) by the relation:

$$\Delta G(T) = \Delta H_{cal}(1-T/T_m) + \Delta Cp(T-T_m) - T\Delta Cp \ln (T/T_m)$$

using ΔCp = 8.47 kcal mol^{-1} K^{-1} as determined experimentally for AHA (44).
Dashed, estimation of PPA stability from its irreversible unfolding parameters.

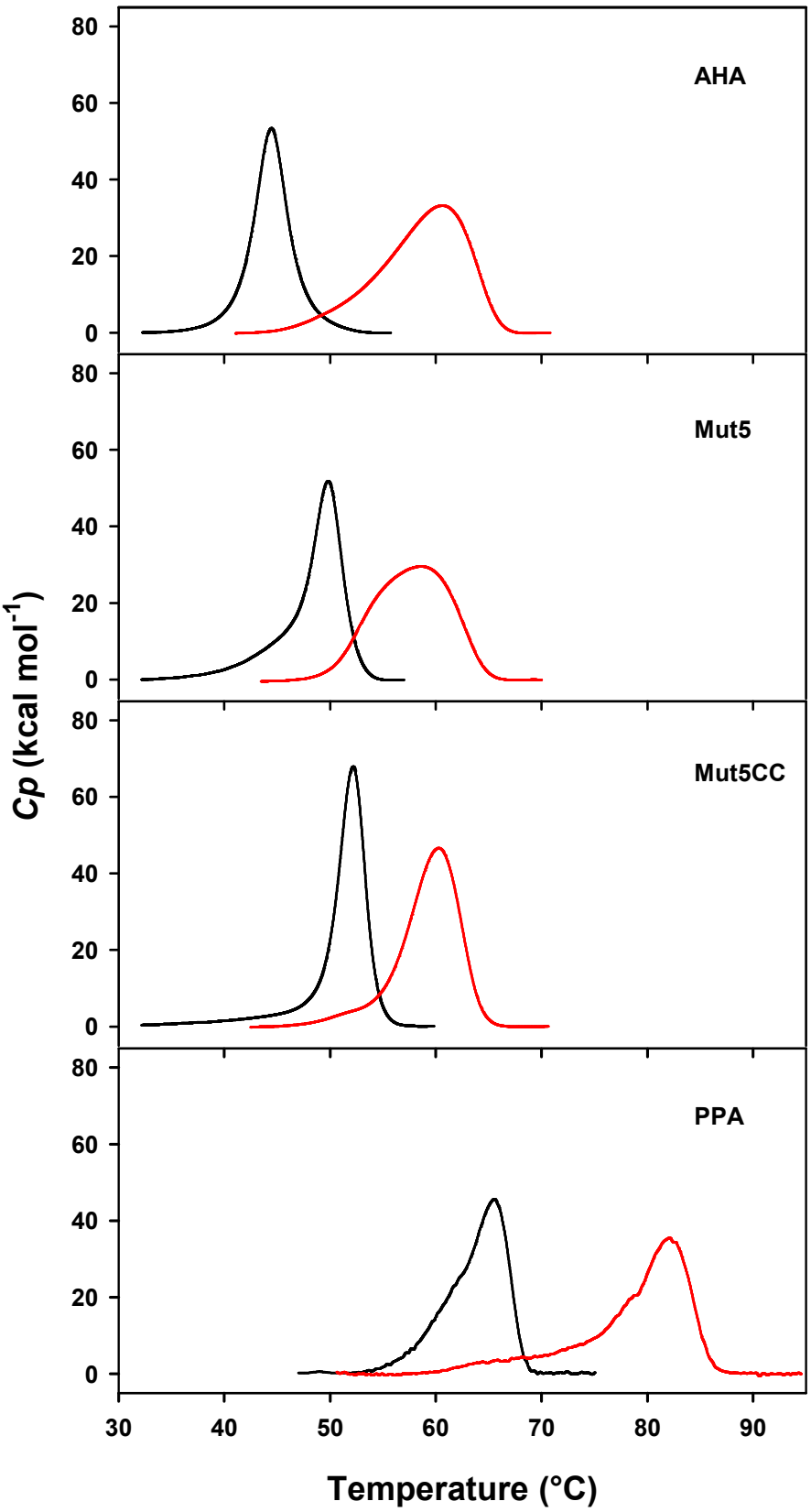

Supplemental Figure S5: Stability of α-amylase-acarbose complexes. DSC endotherms of α-amylases in the free state (black lines) and in complex with the transition state analog acarbose (red lines). T_{max} corresponds to the top of the transition and ΔH_{cal} to the surface below the transition (Table S2). Baseline subtracted data have been normalized for protein concentration.

Supplemental TABLE S2

Microcalorimetric parameters of thermal unfolding for α-amylases in the free state and in complex with the pseudosaccharide inhibitor acarbose.

	Free enzyme		Enzyme-acarbose complex		ΔT_{max}	$\Delta\Delta H_{cal}$
	T_{max} °C	ΔH_{cal} kcal mol^{-1}	T_{max} °C	ΔH_{cal} kcal mol^{-1}	°C	kcal mol^{-1}
AHA	44.0	214	60.6	329	16.6	115
Mut5	49.4	229	58.4	282	9.0	53
Mut5CC	51.8	277	60.1	293	8.3	16
PPA[a]	65.6	295	81.9	306	16.3	11

[a] data from (22)